Full Paper

Journal of the Brazilian Chemical Society

https://dx.doi.org/10.21577/0103-5053.20250035

*J. Braz. Chem. Soc.* **2025**, *36*, 6, e-20250035, 1-14


# Aflavinine Alkaloids from *Aspergillus* sp.: Antibacterial Activity and Inosine 5'-Monophosphate Dehydrogenase (IMPDH) as a Potential Target in *Bacillus subtilis*

***João Victor Silva-Silva,*** [#,a] ***André O. Feitosa,*** [#,b] ***Thiago Henrique Doring,*** [a,c] ***Luciano A. Watanabe,*** [b] ***José Edson S. Siqueira,*** [b] ***Adriano D. Andricopulo,*** [a] ***Patrícia S. B. Marinho*** [b] ***and Andrey Moacir R. Marinho*** [*,b]

[a]*Laboratório de Química Medicinal e Computacional, Instituto de Física de São Carlos, Universidade de São Paulo, 13563-120 São Carlos-SP, Brazil*

[b]*Programa de Pós-Graduação em Química, Universidade Federal do Pará, 66075-110 Belém-PA, Brazil*

[c]*Departamento de Ciências Exatas e Educação, Universidade Federal de Santa Catarina, 89036-002 Blumenau-SC, Brazil*

The search for antimicrobial compounds faces growing challenges due to resistance of bacteria to existing drugs. This study focuses on exploring *Aspergillus* sp. extracts from soil fungi as a valuable source of new lead compounds for drug discovery. Two aflavinine alkaloids isolated from mycelium methanolic extracts were tested against *Escherichia coli*, *Pseudomonas aeruginosa*, *Bacillus subtilis*, *Staphylococcus aureus* and *Salmonella typhimurium* bacteria. The compounds were docked with targets from the genus *Bacillus* to assess interactions, and global reactivity descriptors were calculated using density functional theory (DFT). The interactions of the compounds were assessed using molecular docking and dynamics simulations. Alkaloid **1**, with an additional hydroxyl group, showed stronger inhibition of *B. subtilis* than the reference drugs, according to minimum inhibitory concentration (MIC) results. Energetic scores of **1** correlated with experimental results, indicating an electron-donor nature distinct from penicillin and tetracycline. Docking and dynamics studies showed that **1** had strong interactions with the active site of inosine-5'-monophosphate dehydrogenase (IMPDH). The results suggest that aflavinine alkaloids have potential as inhibitors of Gram-positive bacteria, suggesting possible antimicrobial mechanisms via interactions with IMPDH.

**Keywords:** aflavinine alkaloids, *Aspergillus*, IMPDH, density functional theory, molecular docking, molecular dynamic simulation

## Introduction

The urgent need for more effective antibiotics to fight antibiotic-resistant bacteria has prompted extensive research into bioactive compounds. Fungi have gained significant attention in chemical studies due to their remarkable metabolic capacity to produce a wide array of molecules characterized by low molecular weight, complex chemical structures, and high pharmacological potential.[1,2] Moreover, fungi have been recognized as a valuable source of secondary metabolites with antimicrobial properties.[3]

Within the fungal kingdom, the genus *Aspergillus* stands out as a widely distributed group, known for its potent antimicrobial properties attributed to its rich repertoire of alkaloids, terpenes, steroids, and polyketones.[4] Among these secondary metabolites, alkaloids have exhibited notable antimicrobial activity.[5] Alkaloids can be categorized into different classes[6] based on their chemical skeletons, and this structural diversity has demonstrated impressive antimicrobial efficacy against pathogenic bacteria such as *Escherichia coli*, *Staphylococcus aureus*, *S. epidermidis*, and *Streptococcus pneumoniae*.[7,8]

Furthermore, alkaloids have garnered attention for their ability to inhibit inosine 5'-monophosphate dehydrogenase (IMPDH).[9] IMPDH is a crucial enzyme in the purine nucleotide biosynthesis pathway, which is

*e-mail: andrey@ufpa.br
[#]These authors contributed equally to this work.
Editor handled this article: Paulo Cezar Vieira

essential for bacterial growth and survival. Inhibition of IMPDH disrupts nucleotide synthesis, leading to reduced bacterial viability and presenting a promising strategy for overcoming antimicrobial resistance.[10] Understanding the molecular mechanisms through which fungal alkaloids inhibit IMPDH in bacteria is essential for the development of novel therapeutic approaches.

Computational medicinal chemistry approaches have become vital tools for the design of novel therapeutic agents.[11] Beyond expediting the discovery of bioactive compounds, computational methods play a pivotal role in elucidating structure-activity relationships (SAR).[12] Even seemingly small structural modifications, such as the presence or absence of substituent groups, can have significant impact on molecular and physicochemical properties, as well as on biological activity.[13] Structural changes in bioactive ligands can also lead to substantial differences in their binding modes.[14] Consequently, the utilization of computer-aided drug discovery (CADD) methodologies, including molecular docking, molecular dynamics (MD) and density functional theory (DFT), among others, is crucial in the pursuit of new antibacterial drug candidates.[15,16]

Given the immense potential of fungi as sources of antimicrobial drugs, this study aims to evaluate the methanolic extracts of *Aspergillus* sp. biomass and the corresponding antimicrobial properties of the isolated compounds against both Gram-positive and Gram-negative bacteria. Furthermore, *in silico* investigations provided molecular insights into the potential mechanisms of action of these compounds.

## Experimental

### Fungus

Soil samples from the canga area of Carajás Forest, Pará, were collected in 2012 and the fungus FCN08 was isolated using the Clark method.[17] The identification was made at the Institute of Biological Sciences of UFPA through comparison of vegetative and reproductive structures that were compatible with the genus *Aspergillus*. It was not possible to determine the species of the fungus. One strain is deposited in the LaBQuiM (Programa de Pós-Graduação em Química - Universidade Federal do Pará) with the code FCN08[18] Brazil SisGen No. AE8252A.

### Bacteria

Test microorganisms were *Bacillus subtilis* (ATCC 6633), *Escherichia coli* (ATCC 25922), *Staphylococcus aureus* (ATCC 25923), *Salmonella typhimurium* (ATCC14028) and *Pseudomonas aeruginosa* (ATCC 27853), which were obtained from Instituto Evandro Chagas, Belém, PA, Brazil.

### Culture of *Aspergillus* sp. sabouroud medium and isolation of the chemical constituents

The fungus was cultivated in three Erlenmeyer flasks (1000 mL $min^{-1}$) containing 250 mL $min^{-1}$ of sabouraud medium (Kasvi, Roseto degliAbruzzi, Italy) *per* flask. One flask (sabouraud only) was used as control. Small pieces of potato dextrose agar (PDA) (Kasvi, Roseto degliAbruzzi, Italy) containing mycelium of fungus was transferred under sterile conditions to Erlenmeyer flasks previously autoclaved for 15 min at 121 °C and stored for twenty-five days at 25 °C for colony growth. After simple filtration were obtained mycelium and aqueous phase. The mycelium was macerated with methanol (Tedia, Rio de Janeiro, Brazil) given biomass methanolic extract. The *Aspergillus* sp. FCN08 mycelium methanolic extract (1.0 g) was fractionated on Sephadex LH-20 column (GE Healthcare, Piscataway, USA) using methanol as mobile phase giving 5 fractions F1 to F5. Fraction F4 was analyzed using high performance liquid chromatography (HPLC) Alliance e2695 (Waters, Milford, USA), equipped with Waters 2998 photodiode array detector and Sunfire™ prep C18 column (5 µm, 19 × 150 mm), water and acetonitrile ($H_2O$/ACN) (Tedia, Rio de Janeiro, Brazil) in linear gradient 50 to 100% of the ACN for 30 min as mobile phase, flux of 1.0 mL $min^{-1}$ and volume injection of the 20 µL, sample concentration of 1.0 mg $mL^{-1}$, to obtain chromatographic separation condition. Then, the sample was injected to the HPLC-PAD using a Waters 1525 Binary HPLC Pump (Waters, Milford, USA), equipped with Waters 2998 photodiode array detector and Sunfire™ prep C18 column (5 µm, 19 × 150 mm) semi-preparative mode, using same phase mobile elution system of the analytical mode, using flux of 16 mL $min^{-1}$. Then, compounds **1** and **2** were isolated.

### Identification of isolated compounds

Mass spectra (ESIMS) data were acquired using a Waters Acquity TQD instrument (Waters, Milford, USA). Nuclear magnetic resonance (NMR) 1D and 2D spectra were recorded on a Bruker Ascend 400 (Bruker, Fällanden, Switzerland), using solvent signal (chloroform-*d*) as reference. The chemical shifts are given in delta ($\delta$) values and the coupling constants ($J$) in hertz (Hz). Experimental obtained data were compared with the literature.

### Antimicrobial assay

These assays were performed by applying the broth microdilution method, according to the standards described by the Clinical and Laboratory Standards Institute.[19] In 96 well plates were added 100 µL of culture medium brain heart infusion (BHI) (Himedia, Kennett Square, USA), 100 µL of test material and 5 µL of test bacteria at $1.0 \times 10^4$ colony forming units (CFU) $mL^{-1}$, and incubated at 37 °C (24 h). The compounds obtained from the fungal culture were dissolved initially 1 mg in 100 µL of dimethylsulfoxide (Sigma, Darmstadt, Germany) and 900 µL of BHI broth giving 1 mg $mL^{-1}$ for stock solution. The stock solution was diluted at 1000 µM to 9.25 µM to compounds for the test. Bioactivity was recorded as absence of red coloration in the wells after addition of 10 µL 2,3,5-triphenyltetrazolium chloride (Vetec, Rio de Janeiro, Brazil). The microorganisms were then sub-cultured on BHI plates. The activities of test compounds were classified as bacteriostatic or bactericidal effects according to the behavior of the microorganisms in these sub-cultures. Penicillin and tetracycline were used as positive controls; BHI culture medium was used as negative control.

### DFT studies

The 2D structure of the compounds was drawn by MarvinSketch (version 24.3.0)[20] software and were converted into a single database file SMILES. The pre-optimization has been performed using Avogadro (1.2.0 version)[21,22] with Ghemical Force Field up to $\Delta E < 1 \times 10^{-6}$ kJ $mol^{-1}$. The calculations of quantum studies (DFT) were performed to estimate energy values in vacuum phase. Highest occupied molecular orbital (HOMO) and lowest unoccupied molecular orbital (LUMO) and gap (LUMO – HOMO) has been determined on ORCA 5.0.2[23,24] using B3LYP[25] functional and def2-TZVPP[26] basis sets. The molecular orbitals are generated on Chemcraft 1.8.[27]

### ChEMBL database: screening protein targets

The target selection was conducted using the ChEMBL Database,[28] focusing on species of the genus *Bacillus*, based on *in vitro* inhibition results observed for the tested alkaloids. The search was performed in the "Targets" section under the "Bacteria" category, with an emphasis on Gram-positive bacteria.

The initial search identified 64 potential targets for *Bacillus* in the same category, specifically targeting those listed as "single protein". Refinement of these targets involved two key criteria: the presence of co-crystallized ligands in the Protein Data Bank (PDB) and their performance in docking simulations. Only targets with available co-crystallized ligand structures were considered to ensure realistic binding scenarios. Redocking simulations using GOLD (Genetic Optimization for Ligand Docking) v.2024.1.0 software[29] were then performed, applying a strict root mean square deviation (RMSD) criterion of less than 2.0 to ensure docking accuracy.

Following this rigorous selection process, 17 targets for *Bacillus* were chosen. The complete lists of these selected targets are provided in Table S1 (Supplementary Information (SI) section).

### Molecular docking

The aflavinine alkaloids (**1** and **2**) were designed using MarvinSketch 24.3.0,[20] with pH adjustments based on the physiological pH of each selected target (PDB). The structures were optimized using Avogadro 1.2.0[21,22] with the MMFF94 force field, achieving an energy convergence criterion of $dE = 1 \times 10^{-7}$ kJ $mol^{-1}$. The optimized structures were subsequently exported as MOL2 files. The investigation of the binding affinity of ligands (compounds **1** and **2**) involved molecular docking simulations with selected protein targets. The three-dimensional structures of these targets were obtained from the Research Collaboratory for Structural Bioinformatics Protein Data Bank (RCSB PDB).[30] The surface charge distribution of the targets at their respective physiological pH values was determined by employing the adaptive Poisson-Boltzmann solver (APBS) and PDB2PQR servers.[31] These tools were accessed through the PDB2PQR web server, and calculations were performed using the PARSE force field.[32] The molecular docking analysis was carried out using the GOLD v.2024.1.0 software.[29] The docking procedure used ChemPLP (with ASP as rescore), performing 10 independent runs *per* structure. The poses were ranked based on the scoring functions and the dominance observed within the set of poses for each ligand, which were analyzed using Discovery Studio Visualizer v24.1.0.23298 (BIOVIA).[33] A root mean square deviation (RMSD) of less than 2.0 Å was used as the criterion for successful predictions. All water molecules within the enzyme were processed according to the protocol outlined in the PDB reference articles. The identification of the active site was established based on the geometric center of the co-crystallized ligand, creating a spherical grid with a 15 Å radius. The results were analyzed and visualized using Pymol molecular visualization software.[34] Protein-ligand interactions were identified and visualized using the PLIP web server.[35-37]

### Molecular dynamics simulation

After analyzing the ligand interaction diagram, the high-scoring docking complexes of the aflavinine alkaloids (**1** and **2**) were selected according to each docking parameter for the molecular dynamics (MD) simulation. Desmond software[38,39] was used to analyze molecular interactions at different time scales. From the virtual screening, protein-ligand complexes exhibiting the highest docking scores and the dominance observed within the set of poses for each ligand were selected for further analysis. TIP3P water model was used for solvation of the protein-ligand complexes with the cubic water boundary box set to a box size of 10 Å in each direction (X, Y, and Z). Counter ions were added to the complex to neutralize the solvated system. The complex energy was minimized using an OPLS3e force field.[40,41] In the current study, isothermal-isobaric (NPT) ensemble was employed. The molecular dynamics simulation run time was set at 100 ns, with a recording interval of 100 ps and energy of 1.2 ps. Simulation trajectory visualization and three-dimensional structures were emphasized using Maestro[39] graphical interface.

## Results and Discussion

### Isolation and identification of chemical constituents

The mycelium methanolic extract (1.0 g) of the *Aspergillus* FCN08 cultivated in sabouraud medium was fractionated on Sephadex LH-20 column to afford fractions F1 to F5. Fraction F4 (81 mg), analyzed by HPLC (Figure 1), afforded the diterpenes alkaloids **1** (15.6 mg, 98% purity) and **2** (15.2 mg, 97% purity) (Figure 2).

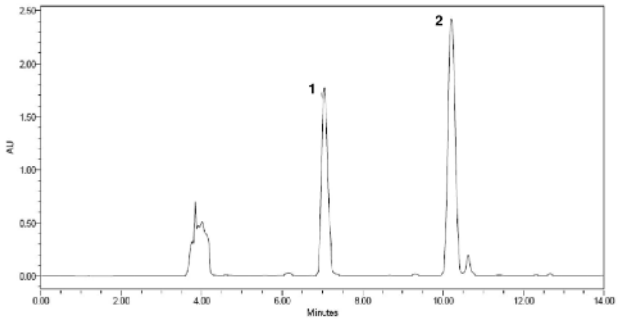


**Figure 1.** Analytical chromatogram of the MeOH extract of fungus FCN08 (sabouraud) at 225 nm. Sunfire C18 column (4.6 × 150 mm, 5 μm); gradient system $H_2O$/ACN 50 to 100% for 14 min, flow 1.0 mL $min^{-1}$, 20 μL sample injected at a concentration of 1 mg $mL^{-1}$.

Compounds **1** and **2** were isolated as white soluble solids in dichloromethane. The ESIMS(−) mass spectrum for **1** showed *m/z* 420 Da, suggesting a molecular formula $C_{28}H_{39}NO_2$. Compound **2** was verified in ESIMS(−) spectrum *m/z* 404 Da, suggesting a molecular formula $C_{28}H_{39}NO$ compatible with the loss of hydroxyl group in comparation to **1**. The $^1$H NMR data for compounds **1** and **2** exhibited a typical pattern of a 3-substituted indole moiety. For compound **1**, signals to aromatic hydrogens were observed at $\delta_H$ 7.53 (d, *J* 8.4 Hz, H-5), $\delta_H$ 7.35 (d, *J* 8.0 Hz, H-8), $\delta_H$ 7.11 (dd, *J* 8.4 and 7.4 Hz, H-6), $\delta_H$ 7.18 (dd, *J* 8.0 and 7.4 Hz, H-7) and $\delta_H$ 7.11 (brs, H-2), these data are characteristics of an indole ring. In the $^{13}$C NMR spectrum, 20 additional carbons can be counted for the molecule, suggesting a terpene moiety, with emphasis on the signals of the methyls Me-26, Me-27, Me-28 and Me-29. Through the heteronuclear multiple bond correlation (HMBC) correlations of H-11 ($\delta_H$ 2.73) a hydroxyl group can be located at C-19 ($\delta_C$ 68.5) and the junction with the indol moiety of the molecule occurs between C-3-C-10. NMR spectra data for compound **2** is similar to compound **1** showing as principal difference at $^1$H NMR the absence of the signal to oxymethinic hydrogen at $\delta_H$ 4.75 and signals arising at $\delta_H$ 0.87 (m, H-14a) and 1.67 (m, H-14b) referring to the $CH_2$ at C-14. The $^1$H and $^{13}$C NMR data for compounds **1** and **2** were compared to literature and were identified as derived of the aflavavin 14-epi-14-hydroxy-10,23-dihydro-24,25-dihydroaflavinin (**1**) and 10,23-dihydro-24,25-dihydroaflavinin (**2**), previously isolated from *Aspergillus tubigensis.*[42] NMR and ESIMS spectra data for compounds **1** and **2** are provided in Table S2 (SI section).

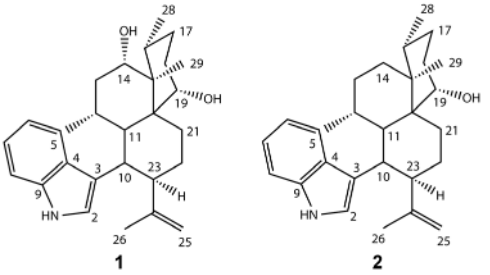


**Figure 2.** Compounds isolated from soil fungi *Aspegillus* sp. FCN08.

Fungi of the genus *Aspergillus* produce a large diversity of the compounds, include alkaloids.[43] Moreover, many species are capable to produce a wide mycotoxins variety, such as aflatoxins, ochratoxins, patulin, citrinin, aflatrem, secalonic acids, cyclopiazonic acid, terrein, sterigmatocystin and gliotoxin.[44,45]

### *In vitro* antimicrobial activity

The diterpene alkaloids **1** and **2**, belonging to a diverse category of natural products, have shown antimicrobial activity against methicillin-resistant *S. aureus* (Table 1).[46]

Compound **1** showed notable activity up to a concentration of 9.25 μM against *B. subtilis*[42] in a disk antimicrobial assay. When tested up to 100 μg *per* disk, an inhibition halo of 15 mm was observed, corroborating our antimicrobial results. Compound **1** also showed good bactericidal activity against *S. aureus* up to minimum inhibitory concentration (MIC) results of 37.05 μM. Compound **2** showed moderate antimicrobial activity against both *B. subtilis* and *S. aureus* with MIC of 308.2 μM, and it was inactive for the other bacteria tested.

The differences observed in antimicrobial activity between Gram-positive and Gram-negative bacteria can be attributed to the distinct structural characteristics of these cells. Gram-positive bacteria have a thick cell wall, primarily composed of peptidoglycan,[47] which facilitates interaction with antimicrobial compounds. In contrast, Gram-negative bacteria possess an additional outer lipid layer,[39] which acts as a protective barrier, hindering the penetration of hydrophobic compounds, such as the tested alkaloids. This structural difference may explain the greater effectiveness of compounds **1** and **2** against *B. subtilis* and *S. aureus*, compared to Gram-negative bacteria, for which the compounds showed limited or no activity. Furthermore, the absence of the hydroxyl group at C-14 may have contributed to the decreased antimicrobial activity of compound **2** compared to **1**. To verify the influence of the hydroxyl group at C-14 on the observed activity, we performed DFT studies, molecular docking, and molecular dynamics simulations with alkaloids **1** and **2**. These studies provided additional insights into how the presence or absence of functional groups can influence the antimicrobial activity of alkaloids and how their interactions with bacterial cells are modulated by molecular structure.

## Quantum studies

DFT is a crucial tool for understanding the electronic properties of molecules and their potential impact on bacterial inhibition.[48] By analyzing the energies of molecular orbitals, such as $E_{HOMO}$ and $E_{LUMO}$, and the electron density distribution in compounds, we gain insights into how electronic interactions affect the ability to inhibit bacteria. This paves the way for promising antimicrobial strategies by manipulating the electronic properties of molecules, including nucleotide biosynthesis.

In the surfaces of the HOMO and LUMO molecular orbitals, obtained via DFT, it is possible to analyze the main collaborations of atomic orbitals. For compound **1**, the main atomic orbitals that collaborate in HOMO are $P_x$ of atoms C15 and C19 and in LUMO, orbital S in C3 and C4. For compound **2**, the main collaborations are $P_x$ for C15, C19 and N18 in HOMO and S in C24, C1, C6 for LUMO. The penicillin presented as main collaborations of atomic orbitals $P_x$ and $P_y$ in C17 and C20 for the HOMO orbital and S in C2, C3, H10 and N13 for the LUMO orbital. Tetracycline presented as main collaborations in the S-type orbital HOMO at C6, C13 and C14 and $P_y$ at N32. For LUMO, S in C2, C14, C15 and C19 featured the biggest collaborations, as can be seen in Figure 3.

HOMO and LUMO energy can be used to determine the formation of charge transfer complexes (CTC), which can elucidate possible drug-receptor interactions.[49] While $E_{HOMO}$ measures the electron donating character of a compound, $E_{LUMO}$ can be used to measure the electron accepting character of chemical structures.[50] The energy values of HOMO, LUMO and gap are presented in Table 2.

DFT studies have demonstrated that the ability to donate electrons grows with $E_{HOMO}$ increasing, which is related to ionization energy. Similarly, the difficulty to receive electrons reduces as $E_{LUMO}$ decreases, which is related to electronic affinity.[51] Compounds **1** and **2** studied have higher LUMO energy values than the reference standards, with a lower receptor potential. However, both studied compounds (**1** and **2**) presented higher $E_{HOMO}$ than the penicillin and tetracycline standards, presenting a more likely electron-donor character. The presence of free electrons in oxygen and nitrogen atoms, in addition to the

**Table 1.** Antimicrobial activity of compounds **1** and **2** isolated from *Aspergillus* sp. FCN08

| Compound | MIC / μM | | | | |
|---|---|---|---|---|---|
| | Gram (+) bacteria | | Gram (–) bacteria | | |
| | *Bacillus subtilis* (ATCC 6633) | *Staphylococcus aureus* (ATCC29213) | *Escherichia coli* (ATCC 25922) | *Pseudomonas aeruginosa* (ATCC 27853) | *Salmonella typhimurium* (ATCC 14028) |
| **1** | 9.25 | 37.05 | > 1000 | > 1000 | > 1000 |
| **2** | 308.2 | 308.2 | > 1000 | > 1000 | > 1000 |
| Penicillin | 23.36 | 23.36 | 23.36 | 23.36 | 23.36 |
| Tetracycline | 17.57 | 17.57 | 17.57 | 17.57 | 17.57 |

MIC: minimum inhibitory concentration; compound **1**: 14-epi-14-hydroxy-10,23-dihydro-24,25-dihydroaflavinin; compound **2**: 10,23-dihydro-24,25-dihydroaflavinin.

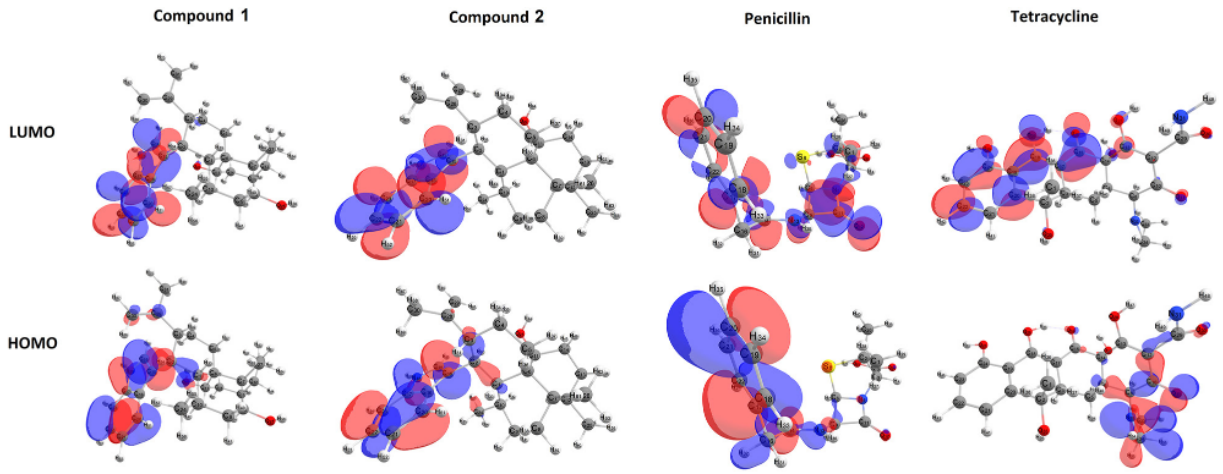


**Figure 3.** Surfaces of HOMO and LUMO to compound **1** (14-epi-14-hydroxy-10,23-dihydro-24,25-dihydroaflavinin), compound **2** (10,23-dihydro-24,25-dihydroaflavinin), penicillin and tetracycline, obtained by DFT method using the def2-TZVPP basis function set and B3LYP functional. In red the positive phases and in blue the negative phases to the orbitals.

**Table 2.** HOMO, LUMO and gap energy values for the studied compounds

| Compound | HOMO / eV | LUMO / eV | Gap / eV |
|---|---|---|---|
| **1** | –5.145 | –0.204 | 4.941 |
| **2** | –5.364 | –0.412 | 4.952 |
| Penicillin | –6.977 | –0.943 | 6.034 |
| Tetracycline | –5.515 | –2.462 | 3.053 |

Compound **1**: 14-epi-14-hydroxy-10,23-dihydro-24,25-dihydroaflavinin; compound **2**: 10,23-dihydro-24,25-dihydroaflavinin; HOMO: highest occupied molecular orbital; LUMO: lowest unoccupied molecular orbital; Gap: (LUMO – HOMO).

indole aromatic system, can potentiate this effect in the biosynthetic compounds reported here.

Collaborations of P-type atomic orbitals are seen in the HOMO of compound **1**, while the region between C1 and C2 has a probability density characteristic of sigma bonding, which is not observed in LUMO. In the HOMO of compound **2**, it is possible to observe a positive phase sigma bonding collaboration between C1 and C2, while the region between C2 and C3 presents a negative phase sigma bonding collaboration, while these collaborations are also not seen in LUMO. HOMO of penicillin presents a probability density concentrated in the phenyl group, while the probability density of LUMO spreads over the entire surface of the structure, with emphasis on the region of the β-lactam ring. While the tetracyclin HOMO presents its probability density in the region of the ring with the amino groups, LUMO occurs mainly in the region of the other three rings.

## Protein targets identified through ChEMBL database screening

Based on the *in vitro* results, compound **1** demonstrated significant antimicrobial activity primarily against Gram-positive bacteria, with particularly promising results against *B. subtilis* compared to the reference drugs. This effectiveness underscores *B. subtilis* as a key target for further research.

To advance the understanding of this activity, molecular targets identified from various species within the genus *Bacillus* using the ChEMBL database are highlighted in Table 3. The identification of molecular targets is essential for developing new antimicrobial therapies, especially in response of growing bacterial resistance. *Bacillus* serves as a crucial model for antibiotic studies due to its diverse resistance mechanisms,[52] highlighting the importance of targets identified through screening in the ChEMBL database.[53] These widely used approaches offer promising opportunities to create innovative antimicrobial therapies that can overcome the limitations of current treatments. The combination of *in vitro* data with molecular target screening is an effective strategy for discovering new therapeutic agents.

## Molecular docking

Molecular docking is a computational method used to predict ligand-target binding poses and affinities, playing a crucial role in virtual screening and drug repurposing. It has significantly accelerated and reduced the cost of drug discovery, particularly in the development of antimicrobial agents, by identifying compounds that inhibit essential microbial proteins.[54,55]

In this study, molecular docking was utilized to examine various *Bacillus* targets, aiming to clarify the *in vitro* inhibition results. The docking analysis revealed that the binding mode scores of the aflavinine alkaloids varied

**Table 3.** *Bacillus* targets identified using the ChEMBL database

| Target | Synonym | Uniprot ID | ChEMBL ID | Organism |
|---|---|---|---|---|
| 1-Phosphatidylinositol phosphodiesterase | PI-PLC | P14262 | CHEMBL4739677 | *B. cereus* |
| Beta-lactamase | blaP | P00808 | CHEMBL5633 | *B. licheniformis* |
| Bifunctional cytochrome P450/NADPH--P450 reductase | cyp102A1 | P14779 | CHEMBL4630872 | *B. megaterium* |
| Dihydrofolate reductase | dfrA | Q81R22 | CHEMBL5270 | *B. anthracis* |
| Dihydroorotase | DHOase | Q81WF0 | CHEMBL3102690 | *B. anthracis* |
| Enoyl-[acyl-carrier-protein] reductase (NADH) | ENR | P54616 | CHEMBL1075044 | *B. subtilis* |
| Erythromycin resistance protein | ermC' | P13956 | CHEMBL4251 | *B. subtilis* |
| Holo-(acyl-carrieir-protein) synthase | acpS | P96618 | CHEMBL4734 | *B. subtilis* |
| Inosine-5'-monophosphate dehydrogenase | IMPDH | A0A6L8P2U9 | CHEMBL3329078 | *B. anthracis* |
| Metallo-beta-lactamase type 2 | blm | P04190 | CHEMBL4295695 | *B. cereus* |
| NH(3)-dependent NAD(+) synthetase | nadE | P08164 | CHEMBL4615 | *B. subtilis* |
| Nicotinate-nucleotide adenylyltransferase | nadD | C3L5T6 | CHEMBL1075320 | *B. anthracis* |
| Peptidoglycan-*N*-acetylglucosamine deacetylase BC_1974 | Bc1974 | Q81EJ6 | CHEMBL4295614 | *B. cereus* |
| Phospholipase C | PLC | P09598 | CHEMBL1293202 | *B. cereus* |
| *S*-Ribosylhomocysteine lyase | luxS | O34667 | CHEMBL5171 | *B. subtilis* |
| Thermolysin | npr | P00800 | CHEMBL3392 | *B. thermoproteolyticus* |
| Tyrosinase | tyr | B2ZB02 | CHEMBL4295634 | *B. megaterium* |

significantly across different targets, highlighting the selective affinity of these compounds for the active sites of *Bacillus* proteins (Table 4).

Among the targets evaluated, inosine-5'-monophosphate dehydrogenase was the only one that showed the best correlation with the *in vitro* results. IMPDH is a critical enzyme in the purine biosynthesis pathway, and its inhibition can have important implications for microbial growth and survival.[10] The molecular docking results for aflavinine alkaloids with IMPDH (PDB ID 4MY1) are

**Table 4.** Scores of the predicted binding modes of aflavinine alkaloids after docking into the active sites of *Bacillus* targets

| Protein | PDB ID | pH | Co-crystalized ligand | | **1** | **2** |
|---|---|---|---|---|---|---|
| | | | RMSD | Score | Score | Score |
| PI-PLC | 1GYM | 7.0 | 0.2365 | 49.83 | 37.24 | 48.11 |
| blaP | 3LY4 | 6.5 | 0.5090 | 56.34 | 47.50 | 50.28 |
| cyp102A1 | 3BEN | 7.4 | 0.5280 | 91.53 | 61.86 | 56.56 |
| dfrA | 4ELF | 7.0 | 0.4168 | 116.55 | 43.62 | 51.07 |
| DHOase | 4YIW | 5.8 | 0.8432 | 69.84 | 55.90 | 44.69 |
| ENR | 3OIG | 7.5 | 0.1648 | 90.80 | 52.80 | 68.12 |
| ermC' | 1QAN | 7.5 | 0.3681 | 87.63 | 41.03 | 36.73 |
| acpS | 1F7L | 7.4 | 0.1194 | 71.58 | 29.78 | 26.95 |
| IMPDH | 4MY1 | 8.0 | 0.3538 | 62.90 | 60.21 | 53.28 |
| blm | 4TYT | 6.5 | 0.2519 | 70.07 | 54.70 | 53.55 |
| nadE | 1IH8 | 8.5 | 0.1919 | 133.83 | 56.61 | 30.22 |
| nadD | 3MLA | 7.5 | 0.5704 | 102.75 | 49.17 | 56.77 |
| Bc1974 | 5N1P | 6.8 | 0.2379 | 48.92 | 41.77 | 33.75 |
| PLC | 1P6D | 7.5 | 0.2866 | 118.82 | 59.41 | 58.11 |
| luxS | 2FQO | 7.0 | 0.1900 | 52.82 | 36.06 | 33.47 |
| npr | 5N3V | 7.5 | 0.2793 | 74.67 | 48.97 | 44.89 |
| tyr | 6EI4 | 7.0 | 0.7907 | 53.62 | 45.60 | 46.82 |

RMSD: root-mean-square deviation; compound **1**: 14-epi-14-hydroxy-10,23-dihydro-24,25-dihydroaflavinin; compound **2**: 10,23-dihydro-24,25-dihydroaflavinin. Score was determined by ChemPLP (with ASP rescore).

presented in Table 5 and Figure 4. The co-crystallized ligand P68, with a score of 62.90, formed hydrogen bonds with residues Glu416-A and Tyr445-C, and hydrophobic interactions with Pro27-C, Leu413-A, and Tyr445-C, indicating a strong affinity and stable complex formation with IMPDH. Alkaloid **1**, with a score of 60.21, also demonstrated significant interactions, forming hydrogen bonds with Lys74-A, Asp251-A, Glu416-A, and Tyr445-C, and hydrophobic interactions with Ala253-A, Leu413-A, and Tyr445-C. In contrast, alkaloid **2**, with a score of 53.28, established hydrogen bonds with Met391-A and Gly392-A, and hydrophobic interactions with Ala253-A, Met391-A, and Glu416-A. Analysis of the protein-ligand complex using the PoseView webserver[56] (Figure 5) revealed π-π stacking interactions between the co-crystallized ligand P68 and compound **1** with residue TYR445-C, which was not observed with compound **2**. These results suggest that **1** has a more favorable interaction profile and a higher potential as a specific inhibitor of IMPDH.

These results demonstrate the robustness and reliability of the alkaloids in interacting with IMPDH, suggesting its potential as a specific inhibitor. The high selectivity

**Table 5.** Interaction of aflavinine alkaloids with the 4MY1 protein

| Compound | Docking score | Hydrogen bonds | | | Hydrophobic interactions | | |
|---|---|---|---|---|---|---|---|
| | | Residue | AA | Distance | Residue | AA | Distance |
| P68 | 62.90 | 416A | Glu | 2.83 | 27C | Pro | 3.90 |
| | | 416A | Glu | 2.86 | 413A | Leu | 3.48 |
| | | 445C | Tyr | 3.98 | 445C | Tyr | 3.68 |
| **1** | 60.21 | 74A | Lys | 3.09 | 253A | Ala | 3.91 |
| | | 251A | Asp | 3.19 | 413A | Leu | 3.24 |
| | | 416A | Glu | 2.88 | 445C | Tyr | 3.59 |
| | | 445C | Tyr | 3.87 | – | – | – |
| **2** | 53.28 | 391A | Met | 2.63 | 253A | Ala | 3.54 |
| | | 392A | Gly | 2.88 | 391A | Met | 3.39 |
| | | – | – | – | 416A | Glu | 2.85 |

AA: amino acids; P68: co-crystallized ligand, 1-(4-bromophenyl)-3-(2-{3-[(1e)-*N*-hydroxyethanimidoyl]phenyl}propan-2-yl)urea; compound **1**: 14-epi-14-hydroxy-10,23-dihydro-24,25-dihydroaflavinin; compound **2**: 10,23-dihydro-24,25-dihydroaflavinin. These interactions were calculated with the Protein-Ligand Interaction Profiler (PLIP) web server.[36] Score was determined by ChemPLP (with ASP rescore).

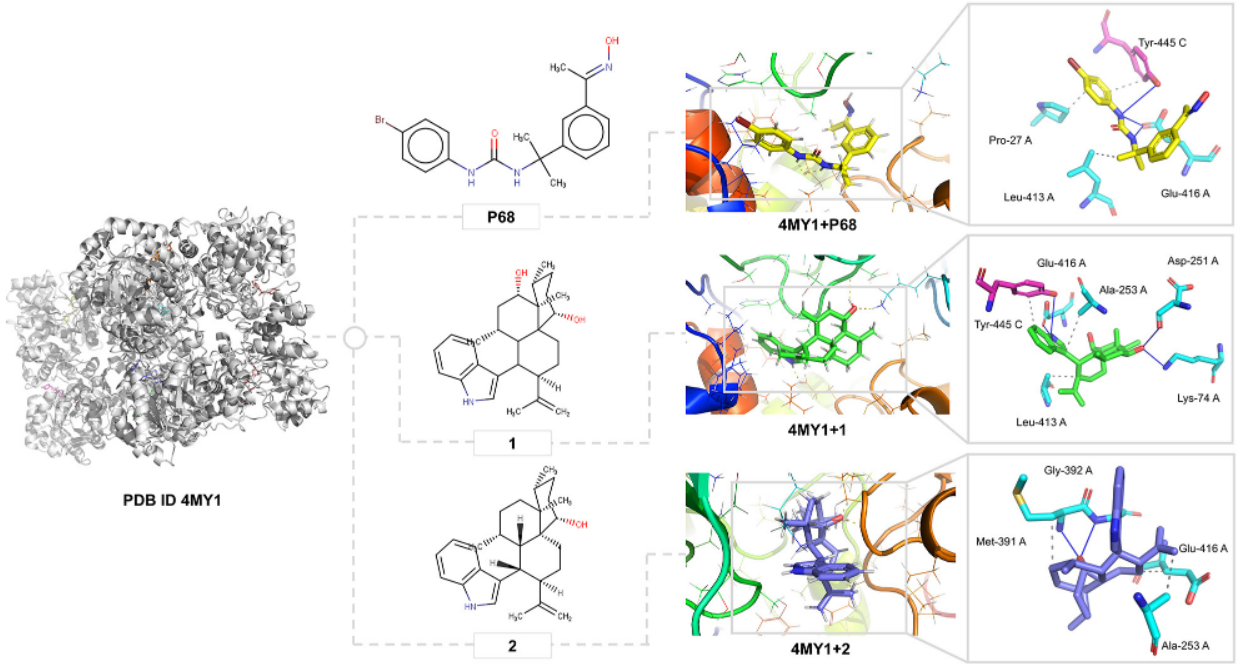


**Figure 4.** Three-dimensional view of the molecular docking show binding interactions of compounds P68 (co-crystallized ligand), **1** and **2** with IMPDH (PDB ID 4MY1).

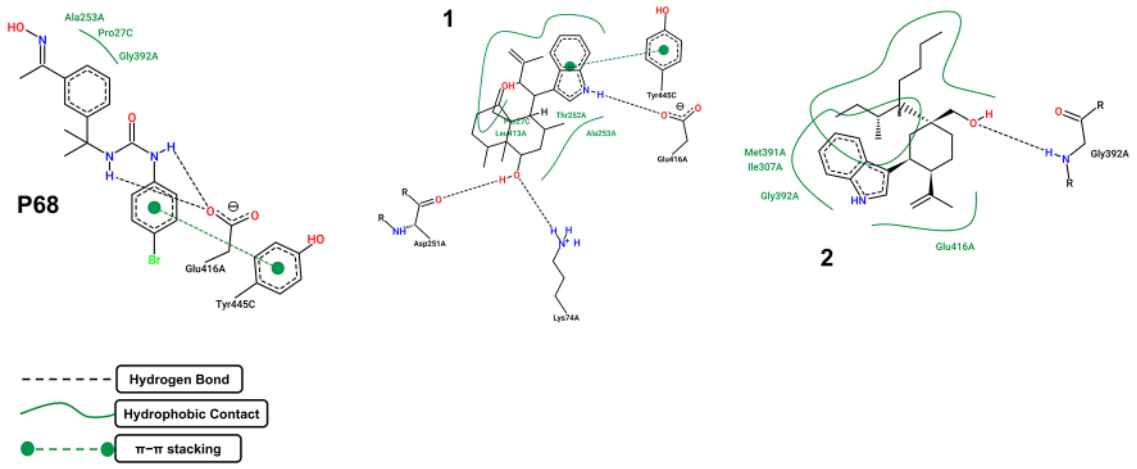


**Figure 5.** 2D representations of binding mode of compounds P68 (co-crystallized ligand), **1** and **2** with IMPDH (PDB ID 4MY1). Figure generated by the Poseview webserver.[56]

of compound **1** characterizes it as a narrow-spectrum antimicrobial,[57] which could benefit the development of targeted treatments by reducing the risk of resistance and minimizing the impact on non-target bacteria, thereby helping to preserve normal microbiota and decrease adverse reactions associated with broad-spectrum antibiotics.[58]

## Molecular dynamic simulation analysis

Molecular dynamics simulation (MD) is an essential tool that provides deep insights into the dynamic behavior of antimicrobial molecules and their interactions with microbial targets, supporting the rational design of new therapeutics. By analyzing the dynamic interactions within antimicrobial-target complexes, MD refines lead compounds and enhances the optimization process, revealing crucial details about antimicrobial mechanisms of action. MD allows researchers to simulate atomic and molecular motions over time, offering valuable information on the structural changes and dynamic processes that occur during ligand-protein interactions.[54]

In this study, the conformational stability and interactions of the IMPDH protein with **1** and **2**, as well as its native ligand (P68, the co-crystallized ligand), were validated through several analyses, including RMSD, root mean square fluctuations (RMSF), interaction profiling, and ligand stability assessments.

In the molecular dynamics analysis of the complexes formed by compound P68 (co-crystallized ligand), **1**, and **2**, significant variations in structural fluctuations and interactions were observed (Figures 6-8, Table 6). The Cα RMSD was highest for **1** (5.06 ± 0.87 Å), compared to P68 (3.87 ± 0.60 Å) and **2** (3.19 ± 0.42 Å), indicating that the protein structure experienced greater fluctuations in the presence of **1**. The ligand RMSD was also higher for **1** (2.57 ± 0.28 Å), compared to P68 (1.55 ± 0.31 Å) and **2** (1.24 ± 0.07 Å), suggesting greater mobility of the ligand within the active site.

In terms of interactions, P68 predominantly formed hydrogen bonds with Glu416-A (88%) and Asp251-A (7%), indicating stable and consistent interactions. Alkaloid **1** primarily interacted with Glu416-A (39%) and Val229-A (20%), whereas alkaloid **2** had predominant interactions with Met391-A (69%) and Gly392-A (28%). The lower percentage of hydrogen bonds for **1**, compared to P68, suggests that these interactions are less stable.

Regarding hydrophobic interactions, P68 demonstrated greater diversity and percentage of interactions, notably with Tyr445-C (29%) and Pro27-C (25%). Although **1** primarily interacted with Leu413-A (32%) and Pro27-C (25%), it showed less diversity in hydrophobic interactions. Alkaloid **2** displayed a more limited range of hydrophobic interactions.

As for π-π interactions, both P68 and **1** formed robust interactions with TYR445-C, observed 97 and 100% of the time, respectively. In contrast, **2** did not show significant π-π interactions.

The RMSD, RMSF, and interaction results suggest that, although **1** exhibited greater mobility and fluctuations during the simulation, it maintained significant and robust interactions with the active site, particularly π-π interactions with Tyr445-C. This suggests that **1** may be a promising IMPDH inhibitor, standing out as a potential antimicrobial agent for *B. subtilis*. In contrast, **2** demonstrated lower stability and affinity, being less efficient in interactions with the active site of the protein.

Table 7 presents the average structural parameters of compound P68 (the co-crystallized ligand), **1**, and **2** from molecular dynamics simulations, including RMSD, radius of gyration (rGyr), molecular surface area (MolSA),

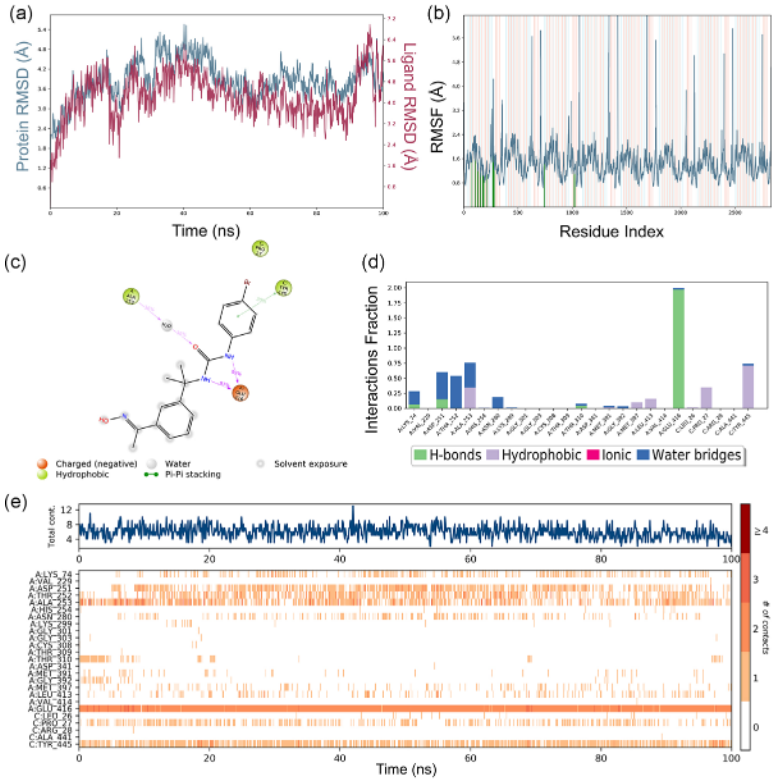


**Figure 6.** MD simulation analysis of the interaction between 4MY1 and P68 (co-crystallized ligand): (a) RMSD (protein RMSD is shown in grey, while RMSD of compound **2** is shown in red), (b) protein RMSF, (c) 2D interaction diagram, (d) protein-ligand contact analysis of the MD trajectory, and (e) protein-ligand contacts over the simulation course.

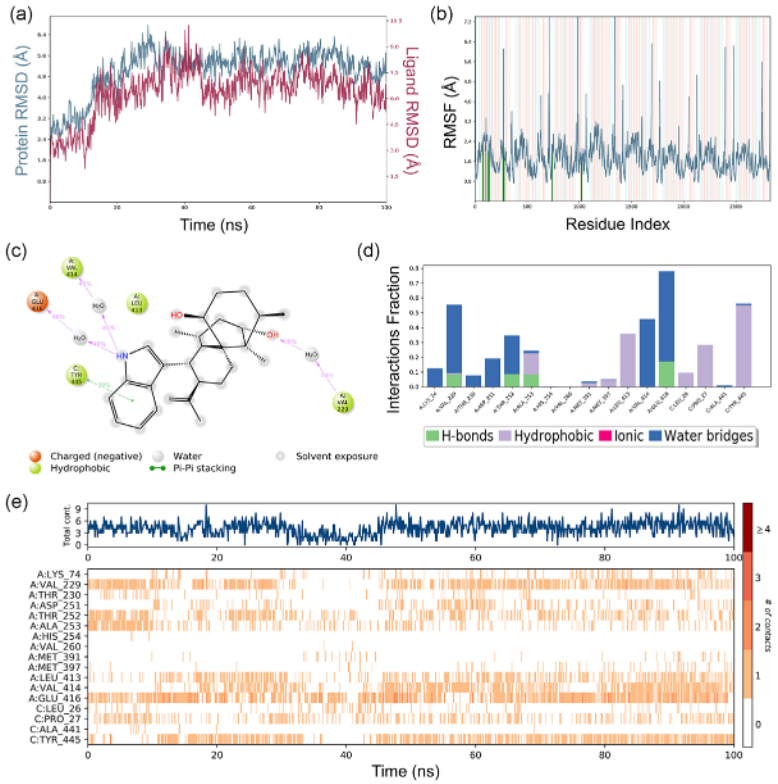


**Figure 7.** MD simulation analysis of the interaction between 4MY1 and compound **1**: (a) RMSD (protein RMSD is shown in grey, while RMSD of compound **2** is shown in red), (b) protein RMSF, (c) 2D interaction diagram, (d) protein-ligand contact analysis of the MD trajectory, and (e) protein-ligand contacts over the simulation course.

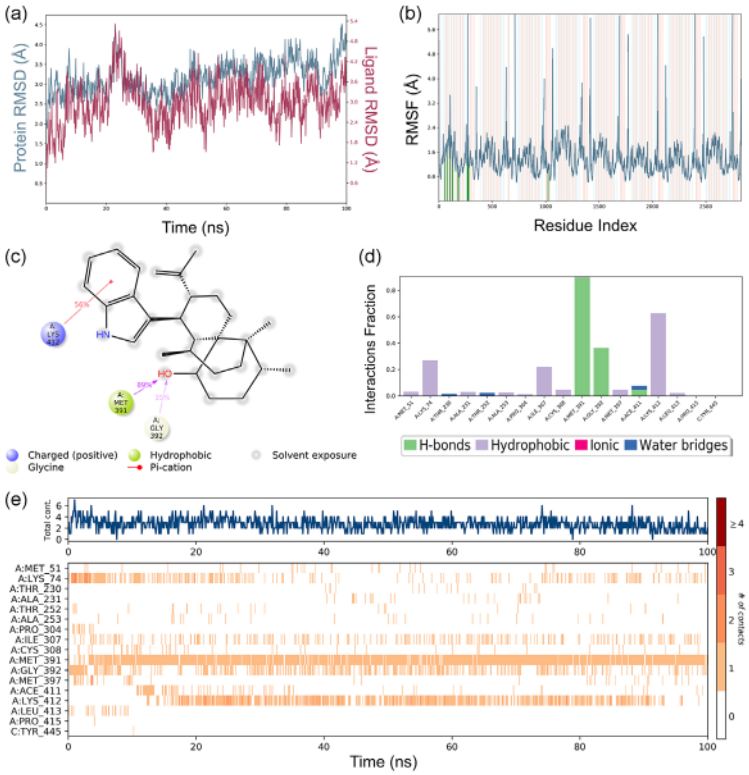


**Figure 8.** MD simulation analysis of the interaction between 4MY1 and compound **2**: (a) RMSD (protein RMSD is shown in grey, while RMSD of compound **2** is shown in red), (b) protein RMSF, (c) 2D interaction diagram, (d) protein-ligand contact analysis of the MD trajectory, and (e) protein-ligand contacts over the simulation course.

solvent accessible surface area (SASA), and polar surface area (PSA).

P68 exhibited an average RMSD of 0.87 ± 0.15 Å, indicating high structural stability. Its rGyr was 4.77 ± 0.08 Å, reflecting a more expanded conformation. The MolSA was 334.73 ± 1.70 Å$^2$, and the SASA was 93.91 ± 18.38 Å$^2$, suggesting moderate solvent accessibility. The PSA was 115.49 ± 2.32 Å$^2$, indicating a significant presence of polar groups.

In contrast, compound **1** demonstrated a lower RMSD of 0.43 ± 0.12 Å, signifying greater structural stability compared to P68. Its rGyr was 3.68 ± 0.04 Å, suggesting a more compact structure. **1** had a MolSA of 363.10 ± 2.20 Å$^2$ and a SASA of 155.75 ± 36.04 Å$^2$, indicating higher solvent accessibility than P68. The PSA was 78.24 ± 3.43 Å$^2$, reflecting fewer polar groups. These attributes suggest that **1** has a higher potential affinity for the target protein, making it a promising IMPDH inhibitor and antimicrobial agent for *B. subtilis*.

With an RMSD of 0.25 ± 0.05 Å, compound **2** demonstrated the highest structural stability among the compounds. Its rGyr was 3.80 ± 0.03 Å, similar to **1**, but with a larger MolSA of 367.39 ± 2.09 Å$^2$ and a smaller SASA of 73.56 ± 18.28 Å$^2$. The PSA was the lowest at 44.80 ± 1.65 Å$^2$, suggesting fewer polar groups and reduced interaction capability with the protein's active site.

Overall, while compound **2** demonstrates superior structural stability, the larger MolSA and SASA of **1** suggest better interaction potential with the target protein. These characteristics underscore the potential of **1** as a more effective IMPDH inhibitor compared to **2**, which, despite its stability, has less favorable interaction properties.

## Conclusions

The chemical analysis of the methanolic extract from the mycelium yielded the aflavinine alkaloids 14-epi-14-hydroxy-10,23-dihydro-24,25-dihydroaflavinin (**1**) and 10,23-dihydro-24,25-dihydroaflavinin (**2**). Alkaloid **1**, which has an additional hydroxyl (OH) group, exhibited significant antimicrobial activity against *B. subtilis* and *S. aureus*, demonstrating superior inhibition of *B. subtilis* compared to the reference drugs, as indicated by the MIC results. Additionally, DFT analysis showed that compounds **1** and **2** have enhanced electron-donor characteristics compared to standard antibiotics like penicillin and tetracycline. Alkaloids demonstrated a better correlation between *in vitro* data and docking results for IMPDH. The docking result interpretation and dynamics simulations provided deeper insights into their

**Table 6.** Averages of RMSD and RMSF values, and interaction percentages for compounds P68 (co-crystallized ligand), **1**, and **2**

| Compound | RMSD / Å | | RMSF | | Hydrogen bonds | Hydrophobic | Water bridge | π-Cation | π- π |
|---|---|---|---|---|---|---|---|---|---|
| | Cα / Å | Ligand / Å | Cα / Å | Ligand / Å | | | | | |
| P68 | 3.87 ± 0.60 | 3.88 ± 0.60 | 1.55 ± 0.31 | 0.39 ± 0.25 | Glu416-A(88%), Asp251-A(7%), Lys74-A(3%), Thr310-A(2%), Thr252-A, Ala253-A, Cys308-A, Gly392-A | Tyr445-C(29%), Pro27-C(25%), Ala253-A(25%), Leu413-A(11%), Met397-A(7%), Leu26-C(1%), Met391-A(1%), Ala441-C | Thr252-A(27%), Asp251-A(23%), Ala253-A(21%), Lys74-A(11%), Asn280-A(9%), Thr310-A(2%), Gly392-A(2%), Tyr445-C(2%), Lys299-A(1%), Met391-A(1%), Glu416-A(1%), Val229-A, His254-A, Gly301-A, Gly303-A, Cys308-A, Thr309-A, Asp341-A, Val414-A, Arg28-C | – | Tyr445-C(97%), His254-A(3%) |
| **1** | 5.06 ± 0.87 | 5.08 ± 0.87 | 2.57 ± 0.28 | 0.17 ± 0.05 | Glu416-A(39%), Val229-A(20%), Thr252-A(20%), Ala253-A(20%), Lys74-A, Thr230-A, Tyr445-C | Leu413-A(32%), Pro27-C(25%), Ala253-A(13%), Tyr445-C(13%), Leu26-C(9%), Met397-A(4%), Met391-A(2%), Val229-A(1%), Val260-A | Glu416-A(27%), Val229-A(21%), Val414-A(21%), Asp251-A(9%), Lys74-A(6%), Thr230-A(3%), Ala253-A(1%), Tyr445-C(1%), His254-A, Met391-A, Met397-A, Ala441-C | – | Tyr445-C(100%) |
| **2** | 3.19 ± 0.42 | 3.21 ± 0.42 | 1.24 ± 0.07 | 0.17 ± 0.06 | Met391-A(69%), Gly392-A(28%), Ace-A411(4%), Thr252-A | Ile307-A(50%), Cys308-A(11%), Met397-A(11%), Met51-A(8%), Ala231-A(6%), Ala253-A(6%), Leu413-A(5%), Pro304-A(3%), Met391-A(2%), Pro415-A | Ace411-A(42%), Thr252-A(31%), Thr230-A(21%), Ala231-A(3%), Lys412-A(3%), Tyr445-C(1%) | Lys74(A)(30%), Lys412(A)(70%) | – |

P68: co-crystallized ligand, 1-(4-bromophenyl)-3-(2-{3-[(1e)-*N*-hydroxyethanimidoyl]phenyl}propan-2-yl)urea; compound **1**: 14-epi-14-hydroxy-10,23-dihydro-24,25-dihydroaflavinin; compound **2**: 10,23-dihydro-24,25-dihydroaflavinin; RMSD: root mean square deviation; RMSF: root mean square fluctuations.

**Table 7.** Average ligand-protein contact diagram of compounds P68 (co-crystallized ligand), **1** and **2**

| Compound | RMSD / Å | rGyr / Å | MolSA / Å | SASA / Å | PSA / Å |
|---|---|---|---|---|---|
| P68 | 0.87 ± 0.15 | 4.77 ± 0.08 | 334.73 ± 1.70 | 93.91 ± 18.38 | 115.49 ± 2.32 |
| **1** | 0.43 ± 0.12 | 3.68 ± 0.04 | 363.10 ± 2.20 | 155.75 ± 36.04 | 78.24 ± 3.43 |
| **2** | 0.25 ± 0.05 | 3.80 ± 0.03 | 367.39 ± 2.09 | 73.56 ± 18.28 | 44.80 ± 1.65 |

P68: co-crystallized ligand, 1-(4-bromophenyl)-3-(2-{3-[(1e)-*N*-hydroxyethanimidoyl]phenyl}propan-2-yl)urea; compound **1**: 14-epi-14-hydroxy-10,23-dihydro-24,25-dihydroaflavinin; compound **2**: 10,23-dihydro-24,25-dihydroaflavinin; RMSD: root mean square deviation; rGyr: radius of gyration; MolSA: molecular surface area; SASA: solvent accessible surface area; PSA: polar surface area.

interaction stability. Specifically, compound **1** exhibited greater mobility and fluctuations but maintained robust interactions with the IMPDH active site. These findings underscore the potential of these bio-synthetic compounds for further antimicrobial research and the development of novel antimicrobial agents.

## Supplementary Information

Supplementary data ($^{1}$H and $^{13}$C NMR spectra, ESI mass spectra for compounds **1** and **2**, and *Bacillus* targets extracted from the ChEMBL Database) are available free of charge at http://jbcs.sbq.org.br as a PDF file.

## Acknowledgments

This research support by the by the Coordination for the Improvement of Higher Education Personnel (Coordenação de Aperfeiçoamento de Pessoal de Nível Superior do Brazil; CAPES), Finance Code 001. João Victor Silva-Silva is a post-doctoral research fellow and scholarship holder, grant number 2023/00242-6, São Paulo Research Foundation (FAPESP). Patrícia S. B. Marinho (CNPq 30863/2021-8) is a productivity scholarship PQ-2. Andrey Moacir do R. Marinho (CNPq 310540/2022-4) is a productivity scholarship PQ-2. Adriano D. Andricopulo (FAPESP grant No. 2013/07600-3) is a productivity scholarship 1A.

### Author Contributions

João V. Silva-Silva was responsible for methodology, investigation, data curation, writing (original draft, review and editing); André O. Feitosa for methodology, investigation, data curation; Thiago H. Doring for methodology, investigation, data curation, writing (original draft, review and editing), conceptualization; Luciano A. Watanabe for methodology, investigation, data curation; José E. S. Siqueira for methodology, investigation, data curation; Adriano D. Andricopulo for conceptualization, supervision, project administration; Patrícia S. B. Marinho for conceptualization, supervision, project administration; Andrey M. R. Marinho for conceptualization, supervision, project administration, resources, formal analysis, validation, writing (original draft, review and editing).

## References

1. Schroeckh, V.; Scherlach, K.; Nützmann, H.-W.; Shelest, E.; Schmidt-Heck, W.; Schuemann, J.; Martin, K.; Hertweck, C.; Brakhage, A. A.; *Proc. Natl. Acad. Sci. U. S. A.* **2009**, *106*, 14558. [Crossref]
2. Avalos, J.; Limón, M. C.; *Encyclopedia* **2021**, *2*, 1. [Crossref]
3. Conrado, R.; Gomes, T. C.; Roque, G. S. C.; De Souza, A. O.; *Antibiotics* **2022**, *11*, 1604. [Crossref]
4. Youssef, F. S.; Alshammari, E.; Ashour, M. L.; *Int. J. Mol. Sci.* **2021**, *22*, 1866. [Crossref]
5. Othman, L.; Sleiman, A.; Abdel-Massih, R. M.; *Front. Microbiol.* **2019**, *10*, 911. [Crossref]
6. Willems, T.; De Mol, M. L.; De Bruycker, A.; De Maeseneire, S. L.; Soetaert, W. K.; *Antibiotics* **2020**, *9*, 340. [Crossref]
7. Zhang, H.; Ruan, C.; Bai, X.; Chen, J.; Wang, H.; *Chem. Nat. Compd.* **2018**, *54*, 411. [Crossref]
8. Liu, Y.-J.; Zhang, J.-L.; Li, C.; Mu, X.-G.; Liu, X.-L.; Wang, L.; Zhao, Y.-C.; Zhang, P.; Li, X.-D.; Zhang, X.-X.; *Molecules* **2019**, *24*, 4596. [Crossref]
9. Abbas, S. A.; Hossain, M. B.; van der Helm, D.; Schmitz, F. J.; Laney, M.; Cabuslay, R.; Schatzman, R. C.; *J. Org. Chem.* **1996**, *61*, 9072. [Crossref]
10. Juvale, K.; Shaik, A.; Kirubakaran, S.; *Med. Chem. Commun.* **2019**, *10*, 1290. [Crossref]
11. Sliwoski, G.; Kothiwale, S.; Meiler, J.; Lowe, E. W.; *Pharmacol. Rev.* **2014**, *66*, 334. [Crossref]
12. Guha, R. In *In Silico Models for Drug Discovery*; Kortagere, S., ed.; Humana Press: Totowa, 2013, p. 81. [Crossref]
13. Lewandowski, W.; Lewandowska, H.; Golonko, A.; Świderski, G.; Świsłocka, R.; Kalinowska, M.; *PLoS One* **2020**, *15*, e0229477. [Crossref]
14. Mobley, D. L.; Dill, K. A.; *Structure* **2009**, *17*, 489. [Crossref]
15. Jukič, M.; Gobec, S.; Sova, M.; *Drug Dev. Res.* **2019**, *80*, 6. [Crossref]
16. Khan, I. M.; Islam, M.; Shakya, S.; Alam, N.; Imtiaz, S.; Islam, Md. R.; *J. Biomol. Struct. Dyn.* **2021**, *40*, 12194. [Crossref]
17. Clark, F. E. In *Methods of Soil Analysis: Part 2 Chemical and Microbiological Properties*, 1st ed.; Norman, A. G., ed.; ASA-SSSA: Madison, USA, 1965, ch. 99, p. 1460-1466. [Crossref]
18. Castellani, A.; *J. Trop. Med. Hyg.* **1967**, *70*, 181.
19. Clinical and Laboratory Standards Institute (CLSI); *CLSI Document M07-A10: Methods for Dilution Antimicrobial Susceptibility Test for Bacteria That Grow Aerobically; Approved Standard*, 10th ed.; CLSI: Wayne, PA, USA, 2015.
20. *MarvinSketch*, version 24.3.0; ChemAxon, Budapest, Hungary, 2024.
21. Hanwell, M. D.; Curtis, D. E.; Lonie, D. C.; Vandermeersch, T.; Zurek, E.; Hutchison, G. R.; *J. Cheminform.* **2012**, *4*, 17. [Crossref]
22. *Avogadro*, version 1.2.0; SourceForge, San Diego, CA, USA, 2021.
23. Neese, F.; *WIREs Comput. Mol Sci*. **2012**, *2*, 73. [Crossref]
24. ORCA, https://orcaforum.kofo.mpg.de/app.php/portal, accessed in February 2025.
25. Lee, C.; Yang, W.; Parr, R. G.; *Phys. Rev. B* **1988**, *37*, 785. [Crossref]
26. Weigend, F.; Ahlrichs, R.; *Phys. Chem. Chem. Phys.* **2005**, *7*, 3297. [Crossref]
27. Zhurko, G. A.; Zhurko, D. A.; *Chemcraft-Graphical Program for Visualization of Quantum Chemistry Computations*; Ivanovo, Russia, 2005.
28. ChEMBL Database, https://www.ebi.ac.uk/chembl/, accessed in February 2025.

29. Cambridge Crystallographic Data Centre (CCDC); *Genetic Optimization for Ligand Docking (GOLD)*, version 2024.1.0; CCDC, Cambridge, Cambs., UK, 2024.
30. Research Collaboratory for Structural Bioinformatics Protein Data Bank (RCSB PDB), http://www.rcsb.org, accessed in February 2025.
31. PDB2PQR web server, https://server.poissonboltzmann.org/pdb2pqr, accessed in February 2025.
32. Dolinsky, T. J.; Czodrowski, P.; Li, H.; Nielsen, J. E.; Jensen, J. H.; Klebe, G.; Baker, N. A.; *Nucleic Acids Res.* **2007**, *35*, W522. [Crossref]
33. *BIOVIA*, version 24.1.0.23298; Dassault Systèmes, Waltham, MA, USA, 2024.
34. *PyMOL*, version 1.8; Schrödinger, LLC, Nova York, USA, 2015.
35. Salentin, S.; Schreiber, S.; Haupt, V. J.; Adasme, M. F.; Schroeder, M.; *Nucleic Acids Res.* **2015**, *43*, W443. [Crossref]
36. PLIP web server, https://plip-tool.biotec.tu-dresden.de/plip-web/plip/index, accessed in February 2025.
37. Adasme, M. F.; Linnemann, K. L.; Bolz, S. N.; Kaiser, F.; Salentin, S.; Haupt, V. J.; Schroeder, M.; *Nucleic Acids Res.* **2021**, *49*, W530. [Crossref]
38. Veeramachaneni, G. K.; Raj, K. K.; Chalasani, L. M.; Bondili, J. S.; Talluri, V. R.; *Drug Des., Dev. Ther.* **2015**, *9*, 4397. [Crossref]
39. *Maestro-Desmond Interoperability Tools*; Schrödinger Release 2021-2; *Desmond Molecular Dynamics System*; Schrödinger, Inc., New York, NY, USA, 2021.
40. Ekhteiari Salmas, R.; Unlu, A.; Bektaş, M.; Yurtsever, M.; Mestanoglu, M.; Durdagi, S.; *J. Biomol. Struct. Dyn.* **2017**, *35*, 1899. [Crossref]
41. Vijayakumar, S.; Manogar, P.; Prabhu, S.; Singh, R. A. S.; *J. Pharm. Anal.* **2018**, *8*, 413. [Crossref]
42. TePaske, M. R.; Gloer, J. B.; Wicklow, D. T.; Dowd, P. F.; *Tetrahedron* **1989**, *45*, 4961. [Crossref]
43. Soltani, J. In *New and Future Developments in Microbial Biotechnology and Bioengineering*; Gupta, V. K., ed.; Elsevier: Amsterdam, 2016, p. 275-292. [Crossref]
44. Navale, V.; Vamkudoth, K. R.; Ajmera, S.; Dhuri, V.; *Toxicol. Rep.* **2021**, *8*, 1008. [Crossref]
45. Pinheiro, E. A. A.; Pina, J. R. S.; Paixão, L. K. O.; Siqueira, J. E. S.; Feitosa, A. O.; Carvalho, J. M.; Marinho, P. S. B.; Marinho, A. M. R.; *Rev. Virtual Quim.* **2018**, *10*, 1438. [Crossref]
46. Tang, M.-C.; Lin, H.-C.; Li, D.; Zou, Y.; Li, J.; Xu, W.; Cacho, R. A.; Hillenmeyer, M. E.; Garg, N. K.; Tang, Y.; *J. Am. Chem. Soc.* **2015**, *137*, 13724. [Crossref]
47. Pasquina-Lemonche, L.; Burns, J.; Turner, R. D.; Kumar, S.; Tank, R.; Mullin, N.; Wilson, J. S.; Chakrabarti, B.; Bullough, P. A.; Foster, S. J.; Hobbs, J. K.; *Nature* **2020**, *582*, 294. [Crossref]
48. Noreen, M.; Rasool, N.; Gull, Y.; Zubair, M.; Mahmood, T.; Ayub, K.; Nasim, F.-H.; Yaqoob, A.; Zia-Ul-Haq, M.; de Feo, V.; *Molecules* **2015**, *20*, 19914. [Crossref]
49. Kumar, A.; Banerjee, K.; Ervasti, M. M.; Kezilebieke, S.; Dvorak, M.; Rinke, P.; Harju, A.; Liljeroth, P.; *ACS Nano* **2021**, *15*, 9945. [Crossref]
50. Miar, M.; Shiroudi, A.; Pourshamsian, K.; Oliaey, A. R.; Hatamjafari, F.; *J. Chem. Res.* **2021**, *45*, 147. [Crossref]
51. Honório, K. M.; Da Silva, A. B. F.; *Int. J. Quantum Chem.* **2003**, *95*, 126. [Crossref]
52. Athamna, A.; Athamna, M.; Abu-Rashed, N.; Medlej, B.; Bast, D. J.; Rubinstein, E.; *J. Antimicrob. Chemother.* **2004**, *54*, 424. [Crossref]
53. Zdrazil, B.; Felix, E.; Hunter, F.; Manners, E. J.; Blackshaw, J.; Corbett, S.; de Veij, M.; Ioannidis, H.; Lopez, D. M.; Mosquera, J. F.; Magarinos, M. P.; Bosc, N.; Arcila, R.; Kizilören, T.; Gaulton, A.; Bento, A. P.; Adasme, M. F.; Monecke, P.; Landrum, G. A.; Leach, A. R.; *Nucleic Acids Res.* **2024**, *52*, D1180. [Crossref]
54. Dalbanjan, N. P.; Praveen Kumar, S. K.; *Indian J. Microbiol.* **2024**, *64*, 879. [Crossref]
55. Muhammed, M. T.; Aki-Yalcin, E.; *Lett. Drug Des. Discovery* **2024**, *21*, 480. [Crossref]
56. Rarey, M.; PoseView Web Server, Proteins Plus; University of Hamburg, Germany, 2025. [Link] accessed in February 2025
57. Alm, R. A.; Lahiri, S. D.; *Antibiotics* **2020**, *9*, 418. [Crossref]
58. Pilmis, B.; Le Monnier, A.; Zahar, J.-R.; *Microorganisms* **2020**, *8*, 269. [Crossref]

*Submitted: November 5, 2024*
*Published online: March 6, 2025*